Design of a new gain-scheduled LPV/Hinf controller for vehicle's global chassis control

Abbas Chokor, Moustapha Doumiati, Reine Talj, Ali Charara

Design of a new gain-scheduled $LPV/\mathscr{H}_\infty$ controller for vehicle's global chassis control *

Abbas Chokor, Moustapha Doumiati, Reine Talj and Ali Charara

Abstract— **This paper investigates new achievements in chassis control. Active Front Steering (AFS) and Direct Yaw Control (DYC) are optimized together to improve -at once- vehicle's maneuverability, lateral stability and rollover avoidance. The novelty of this work with respect to other works in the field of chassis control is that the controller relies on one single centralized approach, where the additive steering angle provided by the AFS and the differential braking provided by the DYC are generated to control the vehicle yaw rate, side slip angle and roll motion. The optimal $\mathscr{H}_\infty$ control technique based on offline Linear Matrix Inequality (LMI) optimal solutions, in the framework of Linear-Parameter-Varying (LPV) systems, is applied to synthesize the controller. A decision making layer instantly monitors two criteria laying on the lateral stability and the rollover. It sends two endogenous weighted parameters, function of the vehicle dynamics, to adapt the controller dynamics and performances according to the driving conditions. The gain scheduled LPV/$\mathscr{H}_\infty$ new control strategy is tested and validated on the professional simulator "SCANeR Studio". Simulations also show the advantage of introducing the roll motion and rollover criteria in the control architecture, comparing to other powerful controllers neglecting these features.**

I. Introduction

A. Motivation

Driving safety is a major challenge for our society. According to the "National Highway Traffic Safety Administration (NHTSA)" statistics, human errors commit almost 90% of road accidents as explained in [1]. The integration of an Advanced Driving Assistance System (ADAS) in the vehicle permits to act in an appropriate way to avoid accidents, skidding and rollover. ADAS systems are formed by several single-actuator approaches, such as: Electronic Stability Program (ESP) or Direct Yaw Control (DYC) to enhance the vehicle lateral stability; Active Front Steering (AFS) to mainly improve the vehicle maneuverability or lane keeping; and (Semi-) Active Suspensions (AS) to improve comfort (roll, pitch and heave motions attenuation), road holding and rollover avoidance.
In the objective of improving the global performance of the vehicle in different driving situations, more sophisticated chassis control systems are developed in literature to create synergies between several ADAS systems. These sophisticated controllers, known as Global Chassis Control (GCC) systems have to deal with the control of complex problems for Multi-Input-Multi-Output (MIMO) systems.

B. Related Works

The coordination between the AFS and the DYC to improve the vehicle maneuverability and lateral stability depending on the driving situation is one of the main tasks in GCC field. Several advanced control methods have been developed for this issue. In a decentralized approach, authors in [2] have developed a DYC controller for lateral stability purpose and an AFS controller for maneuverability purpose, based on sliding mode technique, and then a monitor switches between both stand-alone controllers according to the driving situations. Similarly, based on the fuzzy-logic technique, a coordination approach between AFS and DYC has been developed in [3]. However, the decentralized strategy does not guarantee the internal stability of the system when switching between controllers. [4], [5], and [6] have developed several robust and optimal MIMO centralized controllers based on LPV/$\mathscr{H}_\infty$ control technique, where the $LPV/\mathscr{H}_\infty$ controller penalizes or relaxes the steering and braking to enhance maneuverability and lateral stability. The internal stability of the system is thus guaranteed, since the switching is automated by the controller based on the polytopic approach. However, these controllers does not directly involve the vehicle roll motion and rollover problem in the controller synthesis. Some of them state the advantage on the rollover problem as a consequence of the controller without guaranteeing the rollover avoidance. From the other side, many recent research (centralized and decentralized) such as [7], [8], and [9] propose to control the vertical load transfer, as a function of the roll angle and its angular velocity to avoid rollover. They also conclude the enhancements on lateral stability as a consequence. Nevertheless, these research require the integration of a new actuator into the chassis like (semi-) active suspension or active anti-roll bar. [10], [11] and [12] have developed several powerful centralized $LPV/\mathscr{H}_\infty$ controllers, where the decoupled lateral and vertical vehicle dynamics are respectively controlled by the AFS+DYC and by the (semi-) active suspension. Some other relevant research such as [13], [14], and [15] propose to control the roll motion by the steering and/or braking to avoid the rollover, regardless of the maneuverability and the vehicle trajectory.
All these interesting research have motivated us to study the control of the vehicle yaw rate, the side slip angle and the roll angle to improve vehicle's maneuverability, lateral stability, and rollover avoidance, in a centralized approach, using only steering and braking actuators.

C. This work/contribution

This work exposes the design and validation of a new controller architecture. It combines the control of the yaw rate, the side slip angle, and the roll angle, using only steering and braking actuators, in one single centralized $MIMO\ LPV/\mathscr{H}_\infty$ controller. The global control architecture of the system is shown in Fig. 1. In the control layer, the vehicle yaw rate ψ, the vehicle side-slip angle β, and the suspended mass roll angle θ are the controlled variables. They are fed-back from "SCANeR Studio" vehicle and are optimized together by the $MIMO\ LPV/\mathscr{H}_\infty$ centralized controller, to simultaneously enhance the vehicle maneuverability, the lateral stability and the rollover avoidance. For a good maneuverability, the yaw rate desired trajectory ψ_{ref} is generated by an LTI model called "bicycle model" presented in our previous work [6]. The desired trajectory of β and θ (β_{ref} and θ_{ref} respectively) are set to zero, to minimize them as much as possible.

* This work was supported by the Hauts-de-France Region and the European Regional Development Fund (ERDF).

A. Chokor, R. Talj and A. Charara are with Sorbonne universités, Université de Technologie de Compiègne, CNRS, Heudiasyc UMR 7253, CS 60 319, 60 203 Compiègne, France.

M. Doumiati is with ESEO-IREENA EA 4642, 10 Bd Jeanneteau, 49100 Angers, France.

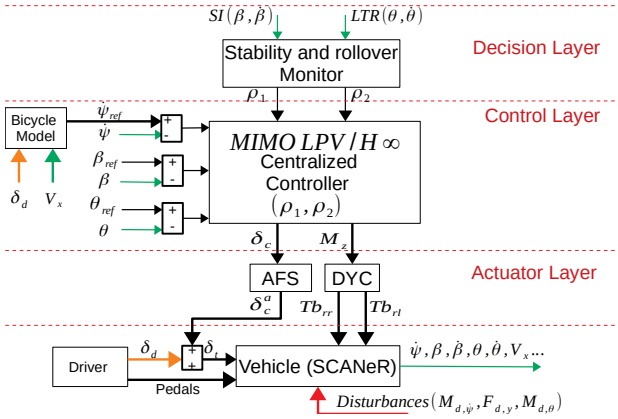

Fig. 1: Global chassis control architecture

Two time-varying scheduling gains/parameters ρ_1 and ρ_2 schedule the *MIMO LPV*$/\mathscr{H}_\infty$ controller objectives. A decision maker (in an upper layer) monitors the vehicle situation and sends instantly the values of the scheduling parameters based on lateral stability (*SI*) and rollover (*LTR*) criteria discussed later. Based on all these information, the *MIMO LPV*$/\mathscr{H}_\infty$ centralized controller generates the control steering angle δ_c and the active yaw moment M_z as the control inputs. In the actuator layer, the Active Front Steering AFS system is formed by an electrical motor that generates the physical control steering called "actuator control steering" δ_c^a that tracks δ_c. AFS provides also the mechanical link between δ_c^a and δ_d, the driver steering angle, where the total steering $\delta_t = \delta_c^a + \delta_d$ (for more information refer to [16]). To prevent direct interference with the active steering on the front tires, the active yaw moment M_z is allocated by the DYC to rear Electro-Mechanical Brakes EMB (right Tb_{rr} and left Tb_{rl}) [5]. AFS and EMB actuators' simplified models are presented later.

This work is an extension of our previous work given in [6]; its originalities with respect to literature are:

- the new control structure, which combines the yaw rate control, the side-slip angle control, and the roll control, in one single centralized controller, ensuring internal stability when switching between maneuverability, lateral stability and rollover avoidance objectives.
- rollover avoidance, lateral stability and maneuverability are guaranteed -a priori- by the controller structure.

The paper structure is as the following: Section II is dedicated to the development of the *MIMO LPV*$/\mathscr{H}_\infty$ centralized controller. We present first the controller structure, then, we detail the linear nominal model used for controller synthesis, the control objectives represented as variable-weighted filters, and finally the *LPV*$/\mathscr{H}_\infty$ controller which guarantees $\mathscr{H}_\infty$ performances between the exogenous inputs and the controlled variables, based on offline LMI optimization, in the framework of the polytopic approach. In Section III, we test and validate the new *LPV*$/\mathscr{H}_\infty$ controller thanks to the co-simulation between Simulink and SCANeR Studio Simulator. We provide also, in the same section, a comparison with the previous *LPV*$/\mathscr{H}_\infty$ developed in [6], which does not include the roll control. Finally, in Section IV, we conclude on the achievements of this work, and provide a glance of our future work.

II. *LPV*$/\mathscr{H}_\infty$ Controller Synthesis

In this section, a detailed description of the global control architecture of Fig. 1 is presented. Notations and vehicle parameters' values used for simulation are given in Table I.

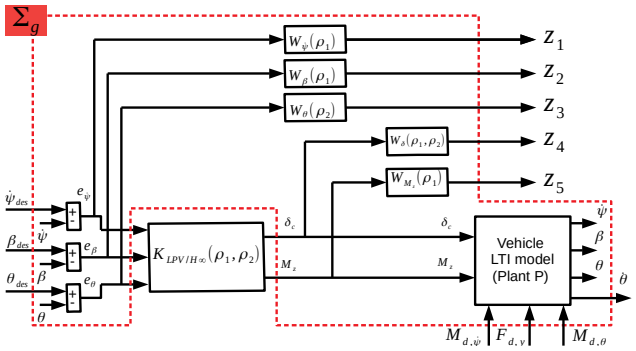

Fig. 2: Control layer architecture

A. Control layer

The control layer architecture is drawn in Fig. 2. As a standard $\mathscr{H}_\infty$ structure, it contains the controller $K_{LPV/\mathscr{H}_\infty}(\rho_1,\rho_2)$ to be synthesized, and the generalized plant $\sum_g$, where ρ_1 and ρ_2 are two endogenous weighted parameters calculated by the decision making monitor to adapt the controller dynamics and performances according to the driving conditions.

The controller $K_{LPV/\mathscr{H}_\infty}(\rho_1,\rho_2)$ has as inputs the errors between the desired trajectories and the actual ones of the yaw rate $e_{\dot{\psi}}$, the side-slip angle e_β, and the roll angle e_θ. Since the $\mathscr{H}_\infty$ approach is a model-based robust control technique, the actual yaw rate, side slip angle, and roll angle are calculated based on a LTI vehicle model represented by the block *"Plant P"* of the generalized plant $\sum_g$.

Plant P has δ_c and M_z as control inputs; $M_{d,\dot{\psi}}$, $F_{d,y}$, and $M_{d,\theta}$ as disturbances (exogenous inputs); and the actual yaw rate $\dot{\psi}$, side slip angle β, and roll angle θ as outputs to be controlled. The vehicle LTI model is a coupled yaw-lateral-roll linear vehicle model, inspired from literature [7], and is given by the following system:

$$\begin{aligned} I_z\ddot{\psi} &= F_{yf}l_f + F_{yr}l_r + I_{xz}\ddot{\theta} + M_{d,\dot{\psi}}, \\ MV\left(\dot{\beta}+\dot{\psi}\right) &= F_{yf} + F_{yr} + M_s h_\theta \ddot{\theta} + F_{d,y}, \\ \left(I_x + M_s h_\theta^2\right)\ddot{\theta} &= M_s h_\theta V\left(\dot{\beta}+\dot{\psi}\right) + (M_s g h_\theta - K_\theta)\theta \\ &\quad - C_\theta\dot{\theta} + M_{d,\theta}, \end{aligned} \tag{1}$$

where F_{yf} represents the lateral force of the front left and right tires merged together at the center of the front axle. Similarly, F_{yr}

TABLE I: Notations and Parameters Values for Simulation

Symbols	Description	Parameters values
θ	Sprung mass roll angle	$[rad]$
ϕ	Sprung mass pitch angle	$[rad]$
$\dot{\psi}$	Vehicle yaw rate	$[rad/s]$
β	Vehicle side slip angle at CG	$[rad]$
F_{y_i}	Lateral forces at the i axle	$[N]$
δ_d	Driver steering angle	$[rad]$
V	Vehicle speed	$[m/s]$
I_x	Roll moment of inertia of sprung mass	534 $[kg.m^2]$
I_z	Vehicle yaw moment of inertia	1970 $[kg.m^2]$
I_{xz}	Vehicle yaw-roll product of inertia	743 $[kg.m^2]$
h_θ	Sprung mass roll arm	0.27 $[m]$
M_s	Sprung mass	1126.4 $[kg]$
t_r	Half rear track	0.773 $[m]$
l_f	Wheelbase to the front	1.0385 $[m]$
l_r	Wheelbase to the rear	1.6015 $[m]$
g	Gravity constant	9.81 $[m/s^2]$
μ	Road adherence coefficient	dry surface= 1 $[-]$
C_f, C_r	Front, rear tire cornering stiffness	76776 $[N/rad]$
K_θ	Roll suspension angular stiffness	30000 $[N.m/s]$
C_θ	Roll suspension angular damper	10000 $[N.m/s]$

is noted for the rear axle. F_{yf} and F_{yr} are given as:

$$\begin{array}{l} F_{yf} = \mu C_f \alpha_f, \\ F_{yr} = \mu C_r \alpha_r, \end{array} \quad (2)$$

and the tires slip angles as:

$$\begin{array}{l} \alpha_f = -\beta - \frac{l_f \dot{\psi}}{V} + \delta_t, \\ \alpha_r = -\beta + \frac{l_r \dot{\psi}}{V}. \end{array} \quad (3)$$

By substituting (3) in (2), and then by substituting (2) in (1), the state space representation of the *Plant P* can be represented by:

$$\begin{array}{l} \dot{X} = AX + B_u U + B_d D, \\ y = X, \end{array} \quad (4)$$

where $X = [\dot{\psi}, \beta, \theta, \dot{\theta}]^T$ is the state vector, $U = [\delta_c, Mz]^T$ is the vector of control inputs, $D = [M_{d,\dot{\psi}}, F_{d,y}, M_{d,\theta}]^T$ is the vector of exogenous inputs. The elements of the state matrix $A \in I\!R^{4\times4}$, and the input matrices $B_u \in I\!R^{4\times2}$ and $B_d \in I\!R^{4\times3}$ are obtained by the same substitutions. The output variables $\dot{\psi}$ and $\dot{\theta}$ are supposed to be measured and given at the CG of the vehicle, in real time control, by a gyrometer; θ is integrated from $\dot{\theta}$ (θ could be directly taken from the Inertial Measurement Unit IMU if available). The side slip angle β, and its velocity $\dot{\beta}$, could be estimated. Several observer approaches that suit the real time constraints implementation and vehicle dynamics have been proposed in literature to estimate β, e.g. an Extended Kalman Filter EKF based observer as done in [11] and [17].

The remaining subsystems of $\sum_g$ i.e. the weighting functions $W_{\dot{\psi}}(\rho_1)$, $W_\beta(\rho_1)$, $W_\theta(\rho_2)$, $W_\delta(\rho_1,\rho_2)$, and $W_{M_z}(\rho_1)$ of Fig. 2 are defined to characterize the performance objectives Z_1, Z_2, and Z_3 and the actuator limitations Z_4, and Z_5 (Dynamics of the actuators, given in Subsection II-C, are neglected during the controller design process). The general form of these weights [6] is given by the following (numerical values are given in the Controller Validation Section, since they depend on the simulated vehicle and integrated actuators):

- $W_{\dot{\psi}}(\rho_1)$ weights the yaw rate signal:

$$W_{\dot{\psi}}(\rho_1) \quad = \quad \rho_1 \frac{s/M_1 + 2\pi f_1}{s + 2\pi f_1 A_1}, \quad (5)$$

where M_1 is sufficiently high for a large robustness margin, and A_1 is the tolerated tracking error on $e_{\dot{\psi}}$. $W_{\dot{\psi}}(\rho_1)$ is shaped to reduce the yaw rate error in the range of frequencies below a roll-off frequency f_1 where the vehicle operates [18]. $W_{\dot{\psi}}(\rho_1)$ is linearly parametrized by the varying parameter ρ_1, where $\rho_1 \in \left\{ \underline{\rho_1} \leq \rho \leq \overline{\rho_1} \right\}$ ($\underline{\rho_1}$ and $\overline{\rho_1}$ are constants representing the lower and higher values of ρ_1). When $\rho_1 = \overline{\rho_1}$, the performance objective $e_{\dot{\psi}}$ is penalized (maneuverability is enhanced), on the contrary, when $\rho_1 = \underline{\rho_1}$, $e_{\dot{\psi}}$ is relaxed (lateral stability becomes a priority).

- $W_\beta(\rho_1)$ weights the side slip angle:

$$W_\beta(\rho_1) \quad = \quad \frac{1}{\rho_1} \frac{s/M_2 + 2\pi f_2}{s + 2\pi f_2 A_2}. \quad (6)$$

M_2, A_2 and f_2 have similar meanings as M_1, A_1 and f_1. $W_\beta(\rho_1)$ is designed similarly to $W_{\dot{\psi}}(\rho_1)$. The main difference is that $W_\beta(\rho_1)$ is inversely dependent on the varying parameter ρ_1. This is because the lateral stability is more promoted than maneuverability in critical situations. This issue is explained later in the decision layer.

- $W_\theta(\rho_2)$ weights the roll angle according to a scheduling parameter ρ_2:

$$W_\theta(\rho_2) \quad = \quad \rho_2 \frac{s/M_3 + 2\pi f_3}{s + 2\pi f_3 A_3}. \quad (7)$$

M_3, A_3 and f_3 have similar meanings as M_1, A_1 and f_1. $W_\theta(\rho_2)$ is linearly parametrized by the varying parameter ρ_2, where $\rho_2 \in \left\{ \underline{\rho_2} \leq \rho_2 \leq \overline{\rho_2} \right\}$ ($\underline{\rho_2}$ and $\overline{\rho_2}$ are constants representing the lower and higher values of ρ_2). When $\rho_2 = \overline{\rho_2}$, the performance objective e_θ is penalized (rollover avoidance is a priority). On the contrary, when $\rho_2 = \underline{\rho_2}$, e_θ is relaxed (rollover is not a risk).

- $W_\delta(\rho_1,\rho_2)$ weights the steering control signal, δ_c:

$$\begin{array}{rcl} W_\delta(\rho_1,\rho_2) & = & (\frac{1}{\rho_1} + \frac{1}{\rho_2}) G_\delta^0 \frac{(s/2\pi f_4 + 1)(s/2\pi f_5 + 1)}{(s/\alpha 2\pi f_5 + 1)^2}, \\ G_\delta^0 & = & \frac{(\Delta_f/\alpha 2\pi f_5 + 1)^2}{(\Delta_f/2\pi f_4 + 1)(\Delta_f/2\pi f_5 + 1)}, \\ \Delta_f & = & 2\pi(f_4 + f_5)/2, \end{array} \quad (8)$$

where $[f_4, f_5]$ is the filter bandwidth. This filter forces the steering system to act at frequencies higher than the driver ones (f_4), to avoid driver annoyance, and lower than the actuator cut-off frequency (f_5). This filter design is inspired from [6]. The novelty here is the dependency of $W_\delta(\rho_1,\rho_2)$ on ρ_1 and ρ_2, which allows to relax or penalize the steering depending on all possible situations. For instance, when rollover stability risk occurs, active steering is promoted to maintain vertical stability, while maneuverability is less achieved and vice versa.

- $W_{M_z}(\rho_1)$ weights the braking, M_z:

$$W_{M_z}(\rho_1) \quad = \quad \rho_1 10^{-5} \frac{s/(2\pi f_6) + 1}{s/(\kappa 2\pi f_6) + 1}, \quad (9)$$

where f_6 is the braking actuator cut-off frequency and κ to handle the braking actuator limitations (see [5]). When $\rho_1 = \overline{\rho_1}$, the braking input is penalized, on the contrary, when $\rho_1 = \underline{\rho_1}$, the braking control signal is relaxed. This design will be related to the vehicle lateral stability.

The controlled outputs Z_1, Z_2, Z_3, Z_4, and Z_5 have to be minimized for any exogenous input. To do so, the powerful $\mathscr{H}_\infty$ control technique is applied here. See [10] and [19] for more information about the robust $(LPV)\mathscr{H}_\infty$ theory.

Interconnection between $\sum_g$ subsystems is done using "*sysic*" Matlab function (Robust Control Toolbox). Since the generalized plant $\sum_g$ is *LPV* [20], it can be formulated as:

$$\Sigma_g(\rho) : \begin{bmatrix} \dot{x} \\ z \\ y \end{bmatrix} = \begin{bmatrix} A(\rho) & B_1(\rho) & B_2(\rho) \\ C_1(\rho) & D_{11}(\rho) & D_{12}(\rho) \\ C_2 & D_{21} & 0 \end{bmatrix} \begin{bmatrix} x \\ w \\ u \end{bmatrix}, \quad (10)$$

where $\rho = \{\rho_1, \rho_2\}$, x includes the state variables of the *Plant P* and of the weighting functions, $w = [\dot{\psi}_{des}, \beta_{des}, \theta_{des}, M_{d,\dot{\psi}}, F_{d,y}, M_{d,\theta}]^T$ is the exogenous input vector, $U = [\delta_c, M_z]^T$ represents the control inputs, $y = [\dot{\psi}, \beta, \theta]^T$ is the measurement vector fed-back to the controller, $y_e = [\dot{\theta}]^T$ is the exogenous output, and $z = [Z_1, Z_2, Z_3, Z_4, Z_5]^T$ is the weighted controlled output vector.

Note that the matrices B_2, and D_{12} depend on ρ, which is not compatible with $\mathscr{H}_\infty$ requirements for polytopic systems. However, this issue is relaxed using some filter on the control input [21].

***Problem resolution:** LMI based LPV/$\mathscr{H}_\infty$:*

The $LPV/\mathscr{H}_\infty$ problem consists in finding the controller $K_{LPV/\mathscr{H}_\infty}(\rho_1,\rho_2)$, scheduled by the parameters ρ_1 and ρ_2, such that:

$$K_{LPV/\mathscr{H}_\infty}(\rho) : \begin{bmatrix} \dot{x_c} \\ u \end{bmatrix} = \begin{bmatrix} A_c(\rho) & B_c(\rho) \\ C_c(\rho) & 0 \end{bmatrix} \begin{bmatrix} x_c \\ y \end{bmatrix}, \quad (11)$$

which minimizes the $\mathscr{H}_\infty$ norm of the closed-loop *LPV* system formed by the interconnection of equations (10) and (11).

Thanks to the Bounded Real Lemma (BRL) extended to LPV systems, this controller can be found. According to system (10) and

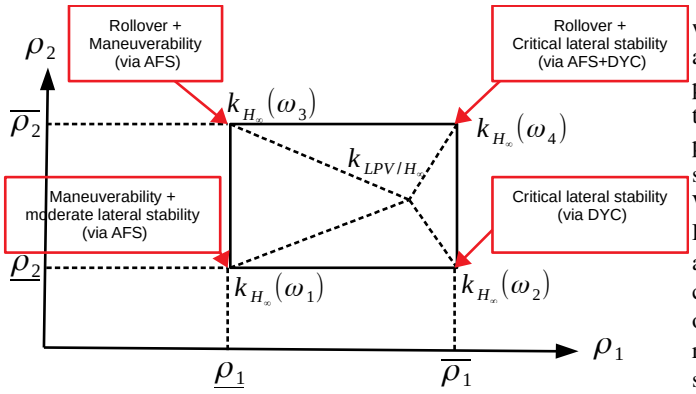

Fig. 3: Controller - Polytopic approach

via the change of basis expressed in [22], a non conservative *LMI* that expresses the same problem as the BRL is formulated in (15) and solved by a Semi-Definite Program (SDP), while minimizing γ for $\rho \in \Omega = [\underline{\rho_1}, \overline{\rho_1}]\ X\ [\underline{\rho_2}, \overline{\rho_2}]$.

The polytopic approach aims at finding $\widetilde{A}$, $\widetilde{B}$ and $\widetilde{C}$ at each vertex of the polytope described by $\rho \in \Omega$, by using a common Lyapunov function, i.e common $X > 0$ and $Y > 0$. Thus, the solution can be obtained by solving the system (12) at each vertex $\left\{\omega_1 = (\underline{\rho_1}, \underline{\rho_2}), \omega_2 = (\overline{\rho_1}, \underline{\rho_2}), \omega_3 = (\underline{\rho_1}, \overline{\rho_2}), \omega_4 = (\overline{\rho_1}, \overline{\rho_2})\right\}$ of the convex hull Ω:

$$\left\{\begin{array}{lcl} C_c(\rho) & = & \widetilde{C}(\rho)M^{-T} \\ B_c(\rho) & = & N^{-1}\widetilde{B}(\rho) \\ A_c(\rho) & = & N^{-1}(\widetilde{A}(\rho) - YA(\rho)X - NB_c(\rho)C_2X \\ & - & YB_2(\rho)C_c(\rho)M^{-T})M^{-T} \end{array}\right. , \quad (12)$$

where $M(\rho)$ and $N(\rho)$ are defined by the user so that $M(\rho)N(\rho)^T = I - X(\rho)Y(\rho)$. See [22] for more details on the computation solution.

According to the polytopic approach, the final controller, $K_{LPV/\mathscr{H}_\infty}(\rho_1, \rho_2)$, is a convex combination of the controllers synthesized at the vertices of the polytope [20] such as:

$$\begin{aligned} K_{LPV/\mathscr{H}_\infty}(\rho_1,\rho_2) = \alpha_1 K_{\mathscr{H}_\infty}(\omega_1) + \alpha_2 K_{\mathscr{H}_\infty}(\omega_2) \\ + \alpha_3 K_{\mathscr{H}_\infty}(\omega_3) + \alpha_4 K_{\mathscr{H}_\infty}(\omega_4), \end{aligned} \quad (13)$$

where $\sum_{i=1}^{i=4} \alpha_i(\rho_1,\rho_2) = 1;\ \alpha_i(\rho_1,\rho_2) > 0$. The polytopic coordinates $\alpha_i(\rho_1,\rho_2)$ weight the controllers on the vertices to construct the final controller, depending on the driving situation, as shown in Fig. 3. $\alpha_i(\rho_1,\rho_2)$ are instantly evaluated by the following equations (the Matlab function"*polydec*" (Robust Control Toolbox) is also useful to evaluate polytopes with more vertices):

$$\begin{aligned} \alpha_1 &= \frac{\overline{\rho_1}-\rho_1}{\overline{\rho_1}-\underline{\rho_1}}.\frac{\overline{\rho_2}-\rho_2}{\overline{\rho_2}-\underline{\rho_2}}; \qquad \alpha_3 = \frac{\overline{\rho_1}-\rho_1}{\overline{\rho_1}-\underline{\rho_1}}.\frac{\rho_2-\underline{\rho_2}}{\overline{\rho_2}-\underline{\rho_2}}; \\ \alpha_2 &= \frac{\rho_1-\underline{\rho_1}}{\overline{\rho_1}-\underline{\rho_1}}.\frac{\overline{\rho_2}-\rho_2}{\overline{\rho_2}-\underline{\rho_2}}; \qquad \alpha_4 = \frac{\rho_1-\underline{\rho_1}}{\overline{\rho_1}-\underline{\rho_1}}.\frac{\rho_2-\underline{\rho_2}}{\overline{\rho_2}-\underline{\rho_2}}. \end{aligned} \quad (14)$$

B. Decision Layer: ρ_1 and ρ_2 calculations

Once the control layer is developed, the decision layer is responsible to monitor the driving situations.

The criterion by which the lateral stability can be quantified is called "*lateral stability index*" *SI*. *SI* reflects the orientation of the vehicle w.r.t its speed vector at the *CG*, and its rate of change. The lateral stability index (SI) used in [11] is expressed in (16) as:

$$SI = \left| q_1\beta + q_2\dot{\beta} \right|, \quad (16)$$

where q_1 and q_2 are estimated depending on the vehicle parameters and road adherence. *SI* varies between 0 and 1. For $SI \leq \underline{SI}$ (a predefined threshold depending on the vehicle and road parameters), the vehicle is in normal driving situations. Thus, the AFS is promoted for maneuverability purpose. It also enhances the lateral stability up to a moderate level. In this range, DYC is penalized. When the vehicle reaches critical lateral stability $SI \geq \overline{SI}$, then the DYC is promoted to enhance the lateral stability. Based on this analysis, the scheduled gain ρ_1 is designed to feed the $LPV/\mathscr{H}_\infty$ controller sufficient knowledge about the weights to be promoted or attenuated. A "*sigmoid*" function (17) (see Fig. 4.a) governs the relation between ρ_1 and *SI*, to ensure a continuous and a relatively smooth variation of ρ_1.

$$\rho_1 = \overline{\rho_1} - \frac{\overline{\rho_1} - \underline{\rho_1}}{1 + e^{-\frac{8}{\overline{SI}-\underline{SI}}(SI - \frac{\overline{SI}+\underline{SI}}{2})}}. \quad (17)$$

The criterion by which the rollover risk is evaluated is called "Load Transfer Ratio" *LTR*. *LTR* reflects vertical load transfer from the inside to the outside wheels w.r.t the corner (turn). An estimation of *LTR* is given in (18) as a function of the roll angle and its rate of change [1]:

$$LTR = r_1\theta + r_2\dot{\theta}, \quad (18)$$

where r_1 and r_2 are estimated depending on the vehicle parameters. *LTR* varies between -1 and 1. When $|LTR| > \overline{LTR}$, where $\overline{LTR}$ a positive constant threshold, a rollover risk is detected, and thus, the controller is informed by the scheduling parameter ρ_2, to handle this risk. To ensure a smooth transition of ρ_2, a lower positive constant threshold $\underline{LTR}$ is defined. A "*sigmoid*" function (19) (see Fig. 4.b) governs the relation between ρ_2 and $|LTR|$.

$$\rho_2 = \underline{\rho_2} + \frac{\overline{\rho_2} - \underline{\rho_2}}{1 + e^{-\frac{8}{\overline{LTR}-\underline{LTR}}(|LTR| - \frac{\overline{LTR}+\underline{LTR}}{2})}}. \quad (19)$$

C. Actuator layer

The Active Front Steering actuator is a controlled electrical motor which provides the additional steering angle δ_c^a. δ_c^a tracks the desired angle provided by the controller δ_c. In order to ensure that controller demand is achievable by the actuator, a simple actuator model is implemented into the control loop of the actuator layer. AFS actuator is modeled as:

$$\dot{\delta}_c^a = 2\pi f_5(\delta_c - \delta_c^a), \quad (20)$$

where f_5 is the actuator cut-off frequency. This actuator is bounded between $\left[-\delta_{c,max}^a, +\delta_{c,max}^a\right]$, where $\delta_{c,max}^a$ is the saturation of the AFS actuator.

The DYC moment M_z is generated as a braking torque $T_{b,rj} = \frac{2r}{t_r}M_z$ at one of the rear wheels of radius r (at the same instant), depending on the direction of M_z [6]. The Electro Mechanical Braking (EMB) actuators providing $T_{b,rj}^a$ (that tracks $T_{b,rj}$) model is given by:

$$\dot{T}_{b,rj}^a = 2\pi f_6(T_{b,rj} - T_{b,rj}^a), \quad (21)$$

where f_6 is the actuator cut-off frequency. This actuator control is bounded between $[0, T_{b,max}^a]$, where $T_{b,max}^a$ is the saturation of the EMB actuators.

III. Controller Validation

This section is dedicated to validate the proposed controller. Validation is done on "SCANeR studio" simulator, by analyzing several vehicle variables on a double lane change test, with the steering angle represented by the variable δ_d on Fig. 12, at an

$$\begin{bmatrix} A(\rho)X + XA(\rho)^T + B_2\widetilde{C}(\rho) + \widetilde{C}(\rho)^T B_2^T & (*)^T & (*)^T & (*)^T \\ \widetilde{A}(\rho) + A(\rho)^T & YA(\rho) + A(\rho)^T Y + \widetilde{B}(\rho)C_2 + C_2^T \widetilde{B}(\rho)^T & (*)^T & (*)^T \\ B_1(\rho)^T & B_1(\rho)^T Y + D_{21}^T \widetilde{B}(\rho)^T & -\gamma I & (*)^T \\ C_1(\rho)X + D_{12}\widetilde{C}(\rho) & C_1(\rho) & D_{11}(\rho) & -\gamma I \end{bmatrix} < 0 \text{ and } \begin{bmatrix} X(\rho) & I \\ I & Y(\rho) \end{bmatrix} > 0. \tag{15}$$

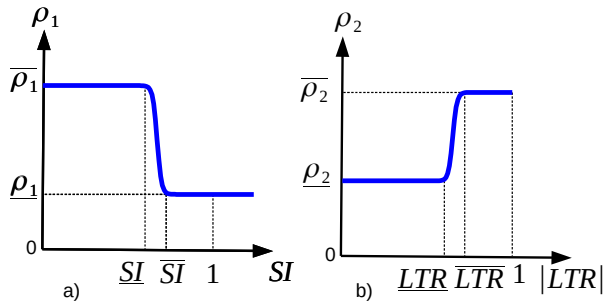

Fig. 4: Scheduling parameters

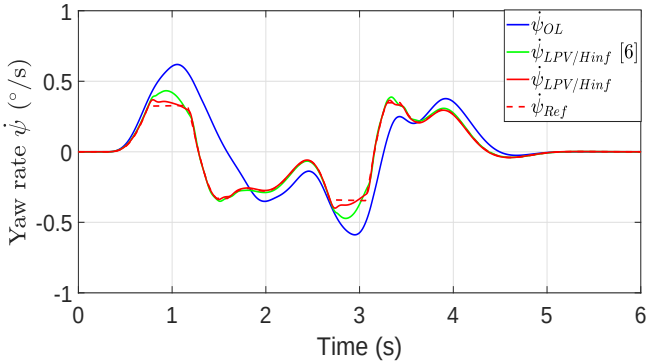

Fig. 5: Yaw rate comparison

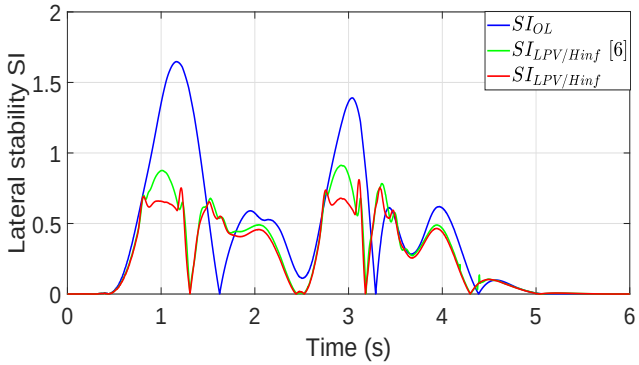

Fig. 6: Lateral stability comparison

initial speed 110 km/h. Comparison is done by integrating the proposed $LPV/\mathscr{H}_\infty$ controller into the vehicle, and comparing it to an uncontrolled vehicle, where the controller is not implemented (OL as Open Loop). Because of the effectiveness of the proposed controller, results are also compared to the $LPV/\mathscr{H}_\infty$ controller of [6] (denoted by "[6]" in the simulations), where the roll angle is not introduced in the controller structure (as many powerful controllers developed in literature and cited in the Related Works Subsection). Numerical values of the controller parameters used in the simulation are provided in Table II.

The yaw rate reference shown in Fig. 5 is generated by the bicycle model. The figure also shows that the proposed $LPV/\mathscr{H}_\infty$ controller has a closest yaw rate to the desired one, compared to the uncontrolled vehicle and the vehicle controlled by the $LPV/\mathscr{H}_\infty$ controller of [6]. However, both controllers have satisfied the maneuverability objective. The small differences at the peak and trough is due to the fact that the $LPV/\mathscr{H}_\infty$ of [6] promotes the lateral stability in this zone, and attenuates the maneuverability objective, because a lateral stability risk appears in this zone as shown in Fig. 6 (green curve). From the other side, the new controller, has a global vision on the system, especially on the roll angle, thus, by detecting a rollover risk, it activates a controller dedicated to rollover and maneuverability (vertex ω_3) as shown by the curve α_3 of Fig. 10. Fig. 8 validates the results by diminishing more the roll angle which reflects enhancements on the Load Transfer Ratio of Fig. 9.

Moreover, the new controller enhances the lateral stability more than the one of [6] as can be seen from Figs. 6 and 7, due to the fourth controller of vertex ω_4 (Fig. 10), which enhances the rollover and lateral stability at once. To summarize, both controllers are able to handle maneuverability and lateral stability objectives. The rollover problem is handled by the $LPV/\mathscr{H}_\infty$ controller of [6] as a consequence of the vehicle lateral control (close to a stable bicycle model as a reference). The advantage of the new controller is the integration of the rollover prevention objective into the controller structure. This feature has added to the new controller the ability to handle more combinations of complex situations like maneuverability and rollover at the same time by using only AFS, and lateral stability and maneuverability at the same time, by using AFS+DYC. This summary is illustrated by the weights α_i of Fig. 10, which correspond to the controllers vertices of Fig. 3. The controller of [6] has only two vertices, which oblige to switch between maneuverability and lateral stability objectives, while, the new controller is able to cover more complex combinations of situations thanks to four vertices controllers.

Fig. 11 shows the fluctuations of the scheduling parameters ρ_1 and ρ_2, based on SI and LTR criteria. To be noted, ρ_2 remains at $\underline{\rho_2}$ the most of the time, this means the rollover risk is rarely detected, and thus, the proposed controller is not totally stimulated, to prove its effectiveness. This issue is due to the fact that lateral stability handling risk appears in passengers cars before rollover risk. Thus, enhancing the lateral stability, will enhance the rollover prevention. The proposed controller could provide more efficient results than the one in [6] for vehicles with higher center of gravity, where rollover risk can be detected at lower values than the lateral stability risk. Fig. 12 shows the driver steering angle δ_d,

TABLE II: Controller Parameters for Simulation

Parameters	Values
$M_1 = M_2 = M_3; A_1 = A_2 = A_3 =; \kappa$	$2; 0.1 = 10\%; 100$
$f_1 = f_2 = f_3; f_4; f_5; f_6$	$11.15\ Hz; 1\ Hz; 10\ Hz; 10\ Hz$
$\underline{\rho_1}; \overline{\rho_1}; \underline{\rho_2}; \overline{\rho_2}$	$70; 85; 75; 85$
$q_1; q_2; r_1; r_2$	$9.55; 2.49; 12; 1$
$\underline{SI}; \overline{SI}; \underline{LTR}; \overline{LTR}$	$0.6; 0.7; 0.6; 0.7$
$\delta^a_{c,max}; T^a_{b,max}$	$5°; 1200\ N.m$

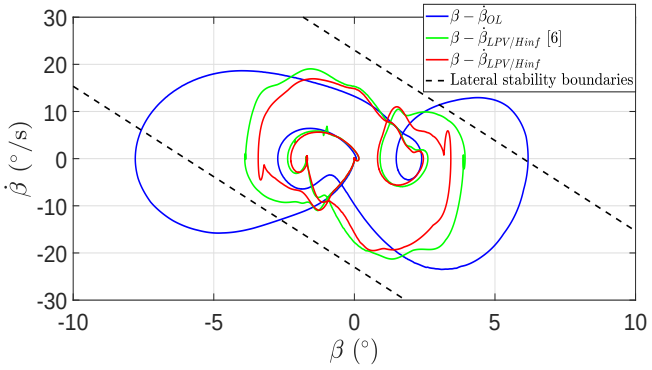

Fig. 7: $\beta - \dot{\beta}$ phase plane

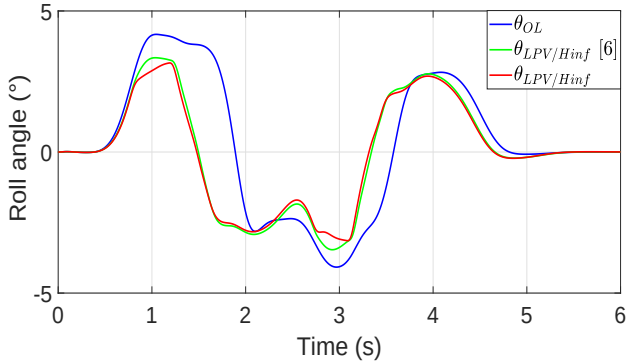

Fig. 8: Roll angle comparison

the AFS steering angle of both controllers δ_c, and the total steering δ_t. One can notice, that both controllers provide similar steering control angles, except at peaks and troughs, where the new proposed controller, actuates more the AFS in order to handle all objectives (the combined complex objectives discussed before). Fig. 13 shows the braking of the EMB at the left and right rear wheels. The new controller less activates the braking with an overall enhancement of the root mean square by 59% at the left braking, and 22% at the right braking. The peak amount of the braking is also reduced by 72% at the left wheel, and 16% at the right wheel. The vehicle speed, which drops due to frictions, is slightly improved as shown in Fig. 14.

IV. CONCLUSION AND PERSPECTIVES

In this paper, a global chassis control architecture has been developed. A decision making layer monitors the stability situation and the rollover risk, then, it sends two endogenous scheduling parameters to a centralized MIMO $LPV/\mathscr{H}_\infty$ controller, in order

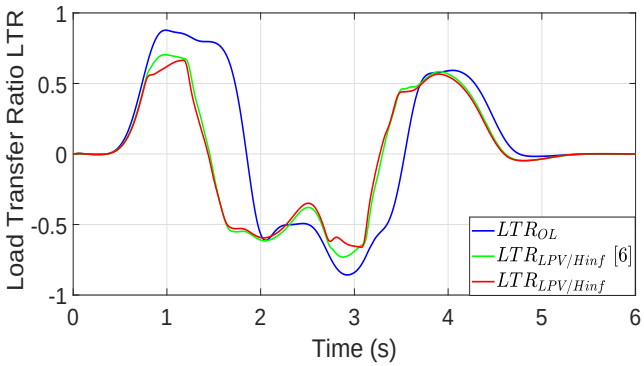

Fig. 9: Load Transfer Ratio comparison

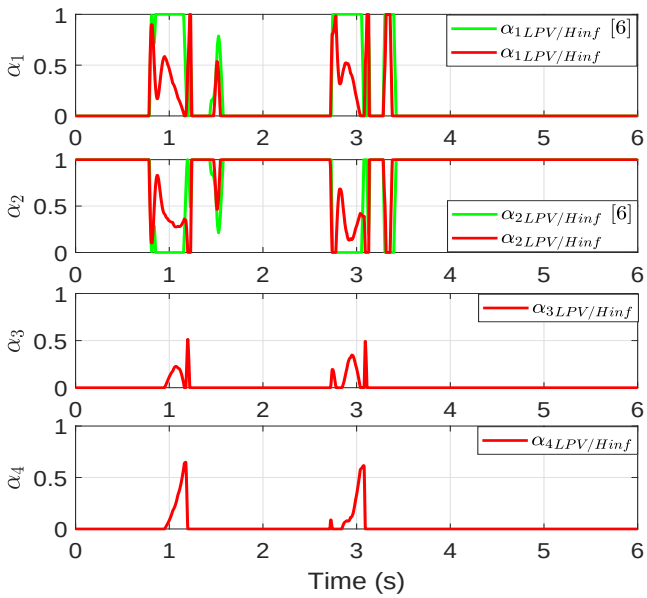

Fig. 10: Weights α_i - vertices controllers

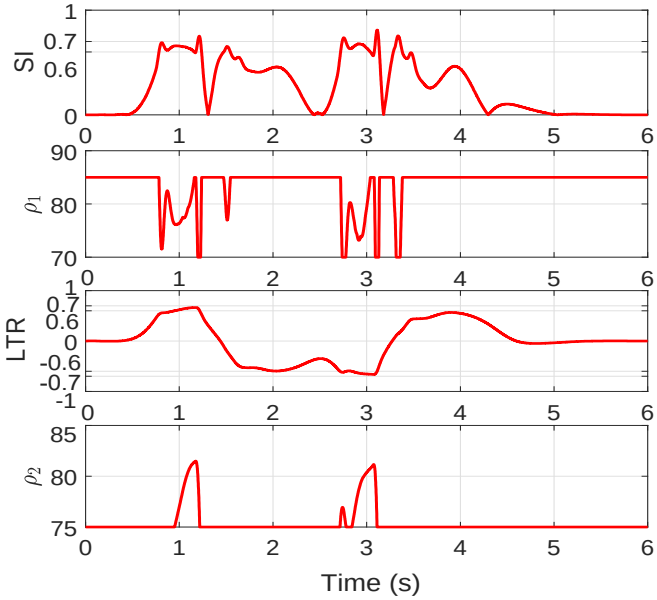

Fig. 11: Decision layer - Inputs vs Outputs

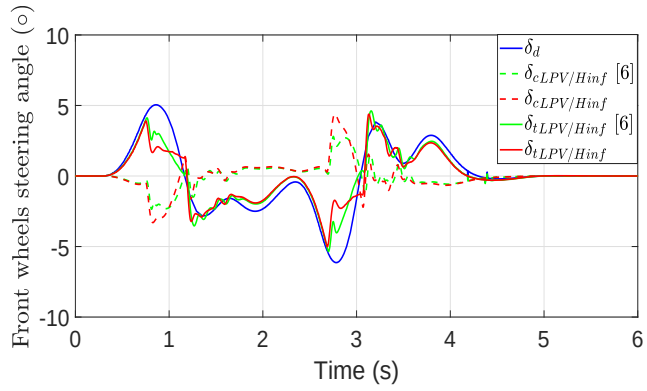

Fig. 12: Steering angle comparison

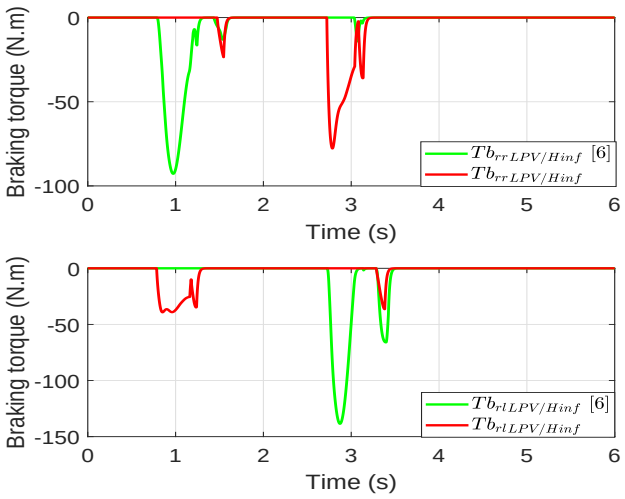

Fig. 13: Braking comparison

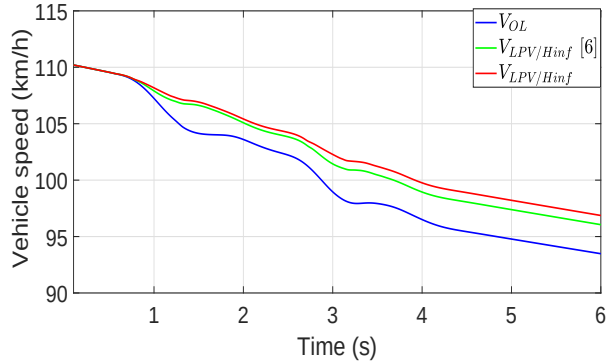

Fig. 14: Vehicle speed comparison

to improve the vehicle maneuverability, the lateral stability and the rollover prevention, by acting on the active front steering and the differential braking. The effectiveness of the proposed controller has been validated on SCANeR Studio simulator compared to an uncontrolled vehicle. The comparison with another $LPV/\mathscr{H}_\infty$ developed in [6], has shown more enhancements by considering the roll angle and rollover risk in the controller synthesis, such as handling more combinations of complex situations.

In the future work, we will further develop the validation of the proposed controller, on a vehicle with higher center of gravity (like SUV). We will also compare this centralized strategy, with a decentralized one, in order to show the pros and cons of each approach, for real-time implementation and validation.

ACKNOWLEDGMENT

The authors would like to thank the Hauts-de-France Region and the European Regional Development Fund (ERDF) 2014/2020 for the funding of this work, through the SYSCOVI project. This work was also carried out in the framework of the Labex MS2T, (Reference ANR-11-IDEX-0004-02) and the Equipex ROBOTEX (Reference ANR-10-EQPX-44-01) which were funded by the French Government, through the program "Investments for the future" managed by the National Agency for Research.

REFERENCES

[1] R. Rajamani, *Vehicle Dynamics and Control*. Springer, 2012.

[2] J. He, D. A. Crolla, M. Levesley, and W. Manning, "Coordination of active steering, driveline, and braking for integrated vehicle dynamics control," *Proceedings of the Institution of Mechanical Engineers, Part D: Journal of Automobile Engineering*, vol. 220, no. 10, pp. 1401–1420, 2006.

[3] R. Karbalaei, A. Ghaffari, R. Kazemi, and S. Tabatabaei, "A new intelligent strategy to integrated control of afs/dyc based on fuzzy logic," *International Journal of Mathematical, Physical and Engineering Sciences*, vol. 1, no. 1, pp. 47–52, 2007.

[4] C. Poussot-Vassal, O. Sename, and L. Dugard, "Robust vehicle dynamic stability controller involving steering and braking systems," in *IEEE European Control Conference (ECC), pp. 3646–3651*, 2009.

[5] M. Doumiati, O. Sename, L. Dugard, J.-J. Martinez-Molina, P. Gaspar, and Z. Szabo, "Integrated vehicle dynamics control via coordination of active front steering and rear braking," *European Journal of Control*, vol. 19, no. 2, pp. 121–143, 2013.

[6] M. Doumiati, A. Victorino, R. Talj, and A. Charara, "Robust lpv control for vehicle steerability and lateral stability," in *53rd IEEE Conference on Decision and Control, pp. 4113–4118*, 2014.

[7] V. T. Vu, O. Sename, L. Dugard, and P. Gáspár, "Enhancing roll stability of heavy vehicle by lqr active anti-roll bar control using electronic servo-valve hydraulic actuators," *Vehicle System Dynamics*, vol. 55, no. 9, pp. 1405–1429, 2017.

[8] J. Yao, G. Lv, M. Qv, Z. Li, S. Ren, and S. Taheri, "Lateral stability control based on the roll moment distribution using a semiactive suspension," *Proceedings of the Institution of Mechanical Engineers, Part D: Journal of Automobile Engineering*, vol. 231, no. 12, pp. 1627–1639, 2017.

[9] M. Mirzaei and H. Mirzaeinejad, "Fuzzy scheduled optimal control of integrated vehicle braking and steering systems," *IEEE/ASME Transactions on Mechatronics*, vol. 22, no. 5, pp. 2369–2379, 2017.

[10] O. Sename, P. Gaspar, and J. Bokor, *Robust control and linear parameter varying approaches: application to vehicle dynamics*. Springer, vol. 437, 2013.

[11] W. Chen, H. Xiao, Q. Wang, L. Zhao, and M. Zhu, *Integrated vehicle dynamics and control*. John Wiley & Sons, 2016.

[12] S. Fergani, O. Sename, and L. Dugard, "A new lpv/h global chassis control through load transfer distribution and vehicle stability monitoring," *IFAC Proceedings Volumes*, vol. 46, no. 2, pp. 809–814, 2013.

[13] J. Ackermann and D. Odenthal, "Robust steering control for active rollover avoidance of vehicles with elevated center of gravity," *Citeseer*, 1998.

[14] D. Odenthal, T. Bunte, and J. Ackermann, "Nonlinear steering and braking control for vehicle rollover avoidance," in *IEEE European Control Conference (ECC), pp. 598–603*, 1999.

[15] S. Solmaz, M. Corless, and R. Shorten, "A methodology for the design of robust rollover prevention controllers for automotive vehicles with active steering," *International Journal of Control*, vol. 80, no. 11, pp. 1763–1779, 2007.

[16] W. Klier, G. Reimann, and W. Reinelt, "Concept and functionality of the active front steering system," SAE Technical Paper, Tech. Rep., 2004.

[17] M. Doumiati, A. Charara, A. Victorino, and D. Lechner, *Vehicle dynamics estimation using Kalman filtering: experimental validation*. John Wiley & Sons, 2012.

[18] B. Heißing and M. Ersoy, *Chassis handbook: fundamentals, driving dynamics, components, mechatronics, perspectives*. Springer Science & Business Media, 2010.

[19] D.-W. Gu, P. Petkov, and M. M. Konstantinov, *Robust control design with MATLAB®*. Springer Science & Business Media, 2005.

[20] P. Apkarian, P. Gahinet, and G. Becker, "Self-scheduled h control of linear parameter-varying systems: a design example," *Automatica*, vol. 31, no. 9, pp. 1251–1261, 1995.

[21] P. Apkarian and P. Gahinet, "A convex characterization of gain-scheduled h/sub/spl infin//controllers," *IEEE Transactions on Automatic Control*, vol. 40, no. 5, pp. 853–864, 1995.

[22] C. Scherer, P. Gahinet, and M. Chilali, "Multiobjective output-feedback control via lmi optimization," *IEEE Transactions on automatic control*, vol. 42, no. 7, pp. 896–911, 1997.